ACS APPLIED MATERIALS & INTERFACES

Research Article

www.acsami.org

Silver Nanoprism Arrays Coupled to Functional Hybrid Films for Localized Surface Plasmon Resonance-Based Detection of Aromatic Hydrocarbons

Laura Brigo,*[,†] Niccolo Michieli,[‡] Luca Artiglia,[§] Carlo Scian,[‡] Gian Andrea Rizzi,[§] Gaetano Granozzi,[§] Giovanni Mattei,[‡] Alessandro Martucci,[†] and Giovanna Brusatin*[,†]

[†]Industrial Engineering Department and INSTM, University of Padova, Padova 35131, Italy

[‡]Department of Physics and Astronomy "Galileo Galilei", University of Padova, Padova 35131, Italy

[§]Department of Chemical Sciences, University of Padova, Padova 35131, Italy

ABSTRACT: We report the achievement of sensitive gas detection using periodic silver nanoprisms fabricated by a simple and low-cost lithographic technique. The presence of sharp tips combined with the periodic arrangement of the nanoprisms allowed the excitement of isolated and interacting localized surface plasmon resonances. Specific sensing capabilities with respect to aromatic hydrocarbons were achieved when the metal nanoprism arrays were coupled in the near field with functional hybrid films, providing a real-time, label-free, and reversible methodology. Ultra-high-vacuum temperature-programmed desorption measurements demonstrated an interaction energy between the sensitive film and analytes in the range of 55−71 kJ/mol. The far-field optical properties and the detection sensitivity of the sensors, modeled using a finite element method, were correlated to experimental data from gas sensing tests. An absorbance variation of 1.2% could be observed and associated with a theoretical increase in the functional film refractive index of ∼0.001, as a consequence to the interaction with 30 ppm xylene. The possibility of detecting such a small variation in the refractive index suggests the highly promising sensing capabilities of the presented technique.

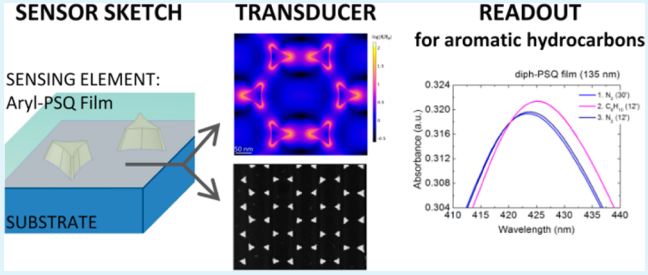

KEYWORDS: *localized surface plasmon resonance, nanoprisms, nanosphere lithography, bridged polysilsesquioxanes, gas sensing, aromatic hydrocarbons*

1. INTRODUCTION

Localized surface plasmon resonance (LSPR) is a nanoscale phenomenon of significant recent interest.[1] A surface plasmon polariton is an optically excited collective oscillation of the free electrons at the surface of a metal. When a surface plasmon is confined to a structure of a size comparable to the wavelength of the incoming light, metal's free electrons participate in the collective oscillation, and a LSPR is excited. The LSPR determines two important effects: (1) the electric fields at the nanostructure's surface are greatly enhanced and rapidly falling off with distance, and (2) the optical extinction has a maximum at the plasmon resonance frequency.[2]

Plasmonic nanostructures allow electromagnetic signal manipulation and information processing on chip for a broad range of applications, primarily chemical and biological sensing.[3,4] In fact, the position and intensity of the optical extinction peak strictly depend on the dielectric properties of the media in which the resonances extend, and such dependence is at the basis of the sensing mechanism.

The implementation of plasmonic nanostructures in micro-sensors on chip has been slowed by the expensive and time-consuming nanofabrication techniques typically employed, based on top-down approaches, such as electron beam lithography. More recently, the diffusion of bottom-up nanofabrication based on nanosphere lithography and self-assembly, combined with subsequent template removal, has provided a simpler, faster, and much cheaper alternative for the creation of plasmonic nanostructures.[5,6] Moreover, this versatile technology allows a rapid on-chip production of plasmonic arrays with packed structures and tunable plasmonic properties.

The development of innovative functional materials for sensitive and selective gas sensing is a very relevant field of current nanotechnology research,[7,8] and great effort is being dedicated to the fabrication of low-cost and efficient nanoscale devices capable of fast and reversible detection. Aromatic hydrocarbons are well-known highly volatile toxic gases, diffusing from contaminated sites in the outdoor air, soil, or groundwater, and indoor pollutants emitted by varnishes or cleaning agents. The American Conference of Governmental Industrial Hygienists (ACGIH) has defined occupational exposure limits of 100, 20, and 0.5 ppm in air for xylene,

Received: February 19, 2014
Accepted: April 21, 2014
Published: April 21, 2014

toluene, and benzene, respectively, as 8 h time-weighted averages.[9]

Among miniaturized aromatic hydrocarbon sensors for *in situ* and real-time detection, resistive electrical devices are the most adopted solutions, but their main drawbacks are the low selectivity, response drift, electromagnetic noise dependence, and need of contact measurements.[10−12] Optical gas sensors, and plasmonic sensors in particular, allow such limits to be overcome and can moreover exhibit thermal and mechanical stability, operate at room temperature, and, as stated above, be integrated on chip.[13,14]

Here we present the design, development, and testing of LSPR-based sensors made of silver (Ag) nanoprism arrays as plasmonic optical transducers, coupled to functional aryl-bridged polysilsesquioxane (aryl-PSQ) films as affinity probes, for fast, sensitive, and reversible detection of aromatic hydrocarbons.

Aryl-PSQs are materials synthesized via a sol−gel process starting from precursors containing two trifunctional silyl groups connected by an aryl bridge, which works as a rigid-rod spacer, conferring controlled porosity[15,16] and specific functionality[17−21] to the hybrid systems. In particular, temperature-programmed desorption investigations of xylene on phenyl-bridged (ph-PSQ) and diphenyl-bridged (diph-PSQ) PSQ films indicate a specific $\pi-\pi$ interaction between the organic component of the films and xylene molecules: the interaction energy has been quantified as 38 ± 14 and 115 ± 13 kJ/mol, respectively.[22]

The sensors are prepared by depositing a thin sol−gel film on an array of Ag nanoprisms fabricated on glass slides through nanosphere lithography. The fabricated substrates were imaged through scanning electron microscopy (SEM), while optical characterization of the substrates and the final sensing systems was performed by UV−vis spectroscopy. To measure the interaction energy between the sensor and analyte, ultra-high-vacuum temperature-programmed desorption (UHV-TPD) measurements of xylene, toluene, and benzene were performed on diphenyl-PSQ films deposited on Ag nanoprism arrays and, as a control system, on the "uncoated" Ag nanoprism arrays.

The sensing performance of such nanostructured systems was tested by monitoring the variation of the LSPRs under exposure to 30 ppm xylene (10 ppm *o*-xylene, 10 ppm *m*-xylene, and 10 ppm *p*-xylene), 30 ppm toluene, or 30 ppm benzene in N_2.

Only a very limited number of plasmon-based sensors for aromatic hydrocarbon detection have been described in the literature.[17,22−24] The distinctiveness of the reported sensors consists of the high sensitivity and the ease of the fabrication procedure, combined with reversibility and fast dynamics.

2. EXPERIMENTAL DETAILS

2.1. Plasmonic Sensor Fabrication, Modeling, and Characterization. The two-dimensional (2D) nanoprism arrays (NPAs) were obtained by the nanosphere lithography technique.[5,25,26] Briefly, a few drops of monodispersed polystyrene nanospheres were deposited on a glass slide. The diameter of the polystyrene nanoparticles was set in the range of 330−520 nm, to tune the LSPR position of the resulting plasmonic nanostructures. The glass slide was then carefully immersed in water in a crystallization vessel. As a result, a monolayer of nanospheres was self-assembled on top of the water, the spheres being organized in a closely packed configuration. Another glass was then used to carefully pick up the monolayer and let it dry in air for 30 min. This procedure yielded large areas (on the order of square centimeters) of the patterned substrate. The ordered domains of the 2D formed crystals extended to several hundreds of square micrometers. Then, to obtain the plasmonic nanoarray, a deposition of Ag was performed by orthogonal thermal evaporation of the metal, up to the desired height, in the range of 50−90 nm. After the deposition, a simple adhesive tape stripping removed the nanospheres together with the residual metal on them. The result was an array of nanoprisms regularly arranged in a honeycomb lattice.

Images of the fabricated plasmonic structures were acquired with a FEG-SEM instrument (model LEO 1530 from Zeiss) operated at an electron energy of 5 kV. The height of the nanoprisms was measured by AFM (model NT-MDT Nova PRO-Solver in noncontact mode).

Electrodynamics simulations were conducted using a finite elements method (FEM)[27] implemented in the commercial software COMSOL Multiphysics, version 4.3b. Nanoprism arrays were modeled by considering the rhombic unit cell (containing two nanoprisms), as shown in Figure 1, and introducing periodic boundary conditions into

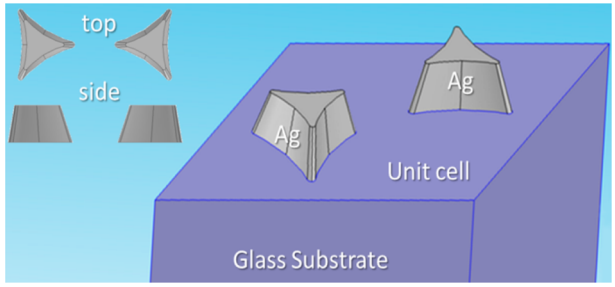

Figure 1. Sketch of the FEM simulation model. The unit cell contains two nanoprisms of Ag supported on the glass substrate. The functional matrix (not shown) was a conformal layer over the substrate and nanoprisms.

the $x-y$ array plane. The size and shape of the nanoprisms were optimized on the basis of the morphological analysis via SEM and AFM. In the z direction, orthogonal to the array plane, the substrate was modeled as semi-infinite; the nanoprisms were placed directly on the substrate.

The active functional layers were modeled as a 135 nm thick conformal coverage of the nanoprisms and substrate. Above the active layer, the medium (air) is semi-infinite. The semi-infinite conditions were necessary to prevent radiation backscattering from the external boundaries: for this purpose, absorbing perfectly matched layer subdomains was considered. The electrodynamics simulation was conducted by solving the Helmholtz equation in the frequency domain. The material properties were described by their complex relative dielectric permittivity function $\varepsilon(\omega)$ and disregarding magnetic effects (relative permeability $\mu_r = 1$ for all the materials). The dielectric functions of Ag and of the functional aryl-PSQ films were collected by spectroscopic ellipsometry measurements, using a J. A. Woollam V-VASE ellipsometer, on flat thin films deposited under the same experimental conditions that were used for the nanoarrays.

2.2. Synthesis of the Functional Material. Aryl-PSQs are organic−inorganic hybrid materials that were synthesized through sol−gel processing. Phenyl-bridged polysilsesquioxanes (ph-PSQ) are obtained starting from a 1,4-bis(triethoxysilyl)benzene monomer (96% pure, Sigma-Aldrich), while diphenyl-bridged polysilsesquioxanes (diph-PSQ) are synthesized starting from 4,4-bis(triethoxysilyl)-1,1-biphenyl (95% pure, Sigma-Aldrich). In both cases, a solution of the sol−gel precursor, ethanol (EtOH), and bi-distilled water was mixed at room temperature in a 1/6 (molar ratio) precursor/H_2O mixture, using 1 N hydrochloric acid (HCl) as the catalyst. The Si−C bonds linking the two ethoxysilanes to the bridging benzenes are hydrolytically stable. A three-dimensional SiO_x network, incorporating benzene rings as network formers, grows as hydrolysis and condensation take place.

The plasmonic sensors were fabricated coating the Ag nanoprism arrays deposited on sodalime slabs with ph-PSQ or diph-PSQ thin films. The sensors were subjected to a postdeposition bake in the

temperature range of 80−200 °C for 30 min. The thickness of the deposited aryl-PSQ films was in the range of 65−200 nm.

Optical absorption spectra of the samples were recorded in the range of 300−900 nm using a JascoV-570 spectrophotometer. The thicknesses of the sensor films were measured using the ellipsometer, acquiring transmittance at normal incidence and ellipsometry quantities (ψ and Δ, respectively) at three different angles of incidence (60°, 65°, and 70°) in the wavelength range of 400−1500 nm, and fitting experimental data with a Cauchy model and Gaussian oscillators for Ag LSPRs. The error in thickness measurements was estimated to be ∼10% and was mainly due to the nonuniformity of the deposition.

A representative absorption spectrum for one of the prepared substrates, before and after coating with a ph-PSQ film, is given in Figure 2 and shows two LSPRs. The main LSPR dipolar band is

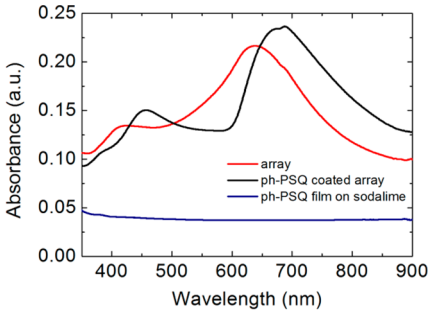

Figure 2. UV−vis absorption spectra of Ag nanoprism arrays obtained using 500 nm diameter polystyrene particles with a 55 nm thick Ag layer on top, before and after coating with a ph-PSQ film. The spectrum of a ph-PSQ film deposited on a sodalime substrate is also shown for comparison.

located at 639 nm, and its position can be red-shifted by the possible interaction between neighboring nanoprisms; the weaker resonance centered at 427 nm is generated by a quadrupolar LSPR resonance of the Ag nanoprisms (as described in the legend of Figure 3). Such resonances undergo a red shift when structures are coated with a thin sol−gel film: the peaks move to 675 and 457 nm, respectively.

2.3. Ultra-High-Vacuum Temperature-Programmed Desorption Measurements. TPD experiments were performed in a multitechnique UHV chamber with a base pressure of 3.0×10^{-10} mbar. The system was equipped with a HIDEN HAL-301 PIC quadrupole mass spectrometer (QMS) with an electron multiplier detector, protected by a quartz shroud.

To perform desorption experiments on the functional system, in a configuration mimicking the actual sensing device, a 10 mm diameter stainless steel support (working as a thermal and electrical conducting support) was coated with a SiO_2 amorphous film obtained by spin coating, using a sol−gel solution synthesized starting from a tetraethoxysilane precursor. Then, an Ag nanoprism array was deposited on the SiO_2 film and then coated with a diph-PSQ film, following the procedures reported in sections 2.1 and 2.2.

The sample was spot-welded to two 0.2 mm diameter Ta wires and connected to a four-degrees of freedom UHV manipulator. A type K thermocouple was spot-welded to the sample rear before the manipulator was mounted in the UHV chamber. The whole system was then pumped and baked at 120 °C for 12 h. Before the experiments were started, a sample degas was performed by heating at 430 K for 10 min. TPD spectra were acquired after the sample had been cooled with a liquid nitrogen flux, exposed to 2.0 L of the aromatic hydrocarbon vapors (1.0 L corresponds to a 1 s dosing time at a pressure of 1.0×10^{-6} Torr), and heated at a rate of 120 K/min. Following this experimental procedure, and considering that the desorption of aromatic hydrocarbons from our sample surface follows first-order kinetics, it was possible to obtain the heat of desorption (ΔE_d) by using the Redhead equation:[28]

$$\Delta E_d = RT_m\left(\ln\frac{\nu_1 T_m}{\beta}\right)$$

where R is the gas constant, T_m is the temperature corresponding to the desorption peak maximum, ν_1 is the frequency factor for the first-order desorption process (we assumed a value of 10^{13} s^{-1}), and β is the linear heating rate, defined as $\beta = dT/dt$.

2.4. Aromatic Hydrocarbon Sensing Measurements. The sensing properties of the fabricated plasmonic systems were tested by mounting the sensors in a gas chamber optically coupled to a UV−vis spectrometer. The incident beam was normal to the surface and illuminated a 9 mm × 1.5 mm sample section. The variation of the LSPRs was monitored under successive cycles of exposure to N_2 (the carrier) and 30 ppm xylene, 30 ppm toluene, or 30 ppm benzene in N_2, with a flow rate of 0.4 L/min.

The response intensity (RI) was evaluated at a fixed λ wavelength of the incident light. The value of λ was chosen to achieve the maximal change in optical absorbance (OAC), defined as the difference between the absorbance measured during analyte exposure and the absorbance during carrier exposure ($OAC = Abs_{analyte} - Abs_{N_2}$). RI was calculated with the equation $RI = |OAC/Abs_{N_2}| = |1 - Abs_{analyte}/Abs_{N_2}|$. The response times ($t_{resp}$) and recovery times ($t_{reg}$) were calculated as the times needed to reach 90% of the total response and reach back 10% of the total response, respectively.

3. RESULTS AND DISCUSSION

3.1. Theoretical Modeling and Characterization of the Plasmonic Sensors. The FEM simulations provided information about both the near-field maps and the far-field properties (scattering and absorption cross sections) of the nanoprism arrays. To assess the performance of the synthesized nanostructures as plasmonic sensors, we conducted a sensitivity analysis.

In Figure 3, a representative near-field map at the main LSPR is reported (Figure 3a) together with the SEM top view of the Ag nanoprism arrays (Figure 3b). The tunability of the plasmonic properties of the NPA is shown in panels c and d of Figure 3 as a function of two geometrical parameters: unit cell side a_0 and nanoprism aspect ratio h_r (defined as the ratio of height to side). The spectra exhibit multipolar resonances whose position can be tuned by controlling the geometrical parameters of the NPA and the level of interaction between the nanoprisms. In general for a given a_0, the increase in the aspect ratio induces a blue shift in the extinction spectra, whereas for a given h_r, a lattice constant increase produces a red-shift of the spectra. The LSPR tunability can be used to tailor the main resonances (dipolar or multipolar) according to the spectral regions more suitable for the sensing setup. At the dipolar LSPR peak, a local field enhancement of ∼2 orders of magnitude at the nanoprism tips is calculated. The field map shows that the nanoprisms are not strongly interacting (the electromagnetic field in the middle of the gap region between neighboring nanoprisms is weak); thus, the possible presence of defects in the 2D lattice does not strongly influence the efficiency of the LSPR. On the other hand, possible small-scale defects on the prisms produced during the metal deposition (such as the presence of a few <5 nm tiny satellite nanoparticles around the nanoprisms on the glass substrate) may lead to additional local hot spots, thus further enhancing the sensing capabilities of the nanostructure. As a consequence, the computed variations should be considered as a lower limit for the performance of the sensors, because by using a more interacting configuration the near-field hot spot can be further increased.

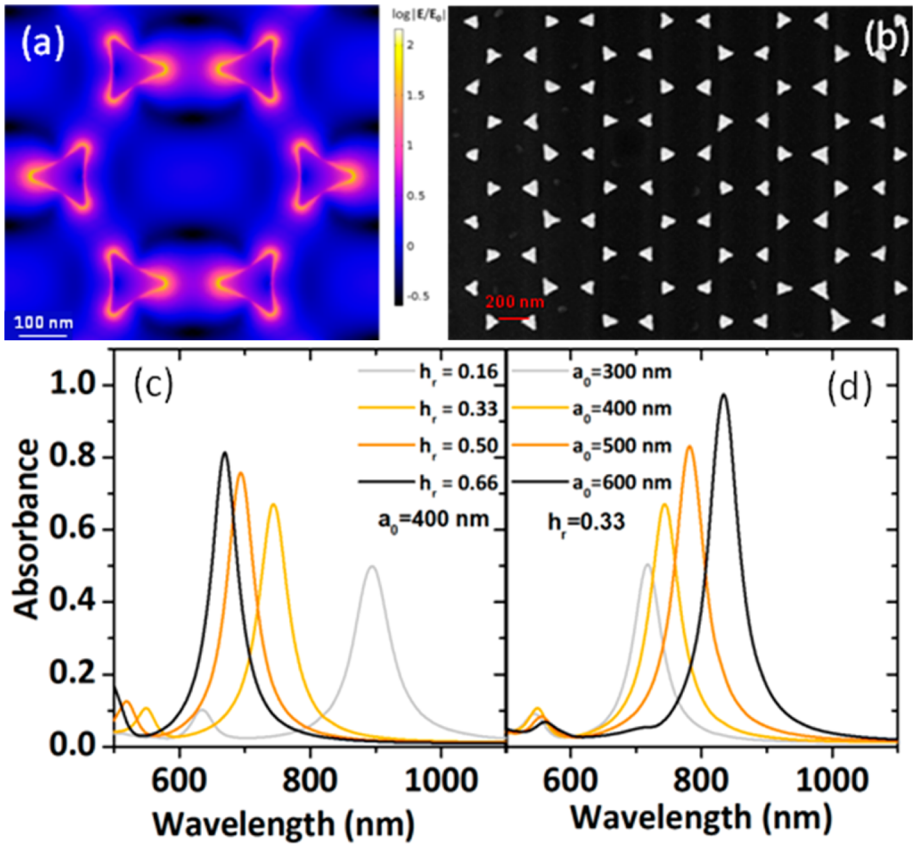

Figure 3. (a) Log of the local field modulus (normalized to the external field E_0) calculated by FEM simulation at the LSPR resonance for an ordered array of Ag nanoprisms deposited on a silica substrate. A local field enhancement of ~2 orders of magnitude is obtained at the nanoprism tips. (b) SEM top view of the Ag nanoprism arrays showing the honeycomb lattice. Far-field calculations as a function of the geometrical parameters of the uncoated NPA: absorbance vs nanoprism aspect ratio, h_r, for a lattice constant a_0 of 400 nm (c) and vs lattice constant a_0 for an h_r of 0.33 (d).

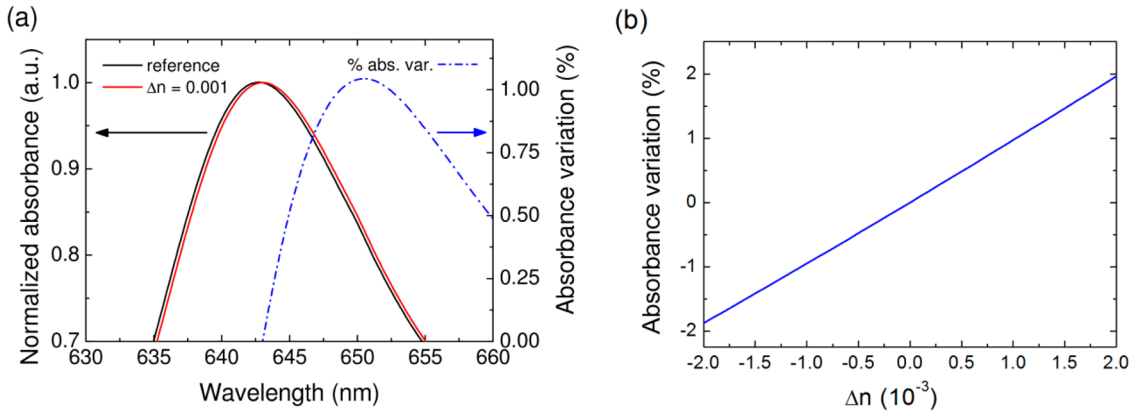

Figure 4. (a) FEM-simulated LSPR peak. The two normalized absorbance curves (left scale) are computed using the refractive index of the functional sol–gel system ("reference", black line) and the same refractive index increased by a Δn of 0.001 (red line). The percent difference (right scale, dotted–dashed line) has its maximum red-shifted by ~10 nm, where the derivative of the curves is the largest. (b) Absorbance variation as a function of the refractive index variation. The relation is linear. The proposed strategy allows in principle the detection of extremely small refractive index changes, i.e., on the order of Δn = 0.001.

The effect of an increase in the refractive index at the surface of plasmonic nanostructures is visible in a red-shifted and slightly enhanced LSPR peak. To check the magnitude of refractive index variation that could in principle be detected by measuring the OAC, the refractive index of the matrix was varied by 0.001, which is the order of magnitude of the refractive index increase possibly induced by the incorporation of the analyte gas in the sol–gel matrices deposited on the Ag nanoprism arrays. In fact, an attempt to experimentally measure a variation in the refractive index of aryl-PSQ films when exposed to 30 ppm xylene was performed via spectroscopic ellipsometry. Such a variation proved to be <0.01, and not measurable because of the resolution limits of the technique. Figure 4a shows the two absorption curves in the region of the LSPR peak at λ = 643 nm, together with their percent difference d, defined as $d(\Delta n) = [A(\Delta n) - A_0]/A_0$.

dx.doi.org/10.1021/am501042f | ACS Appl. Mater. Interfaces 2014, 6, 7773–7781

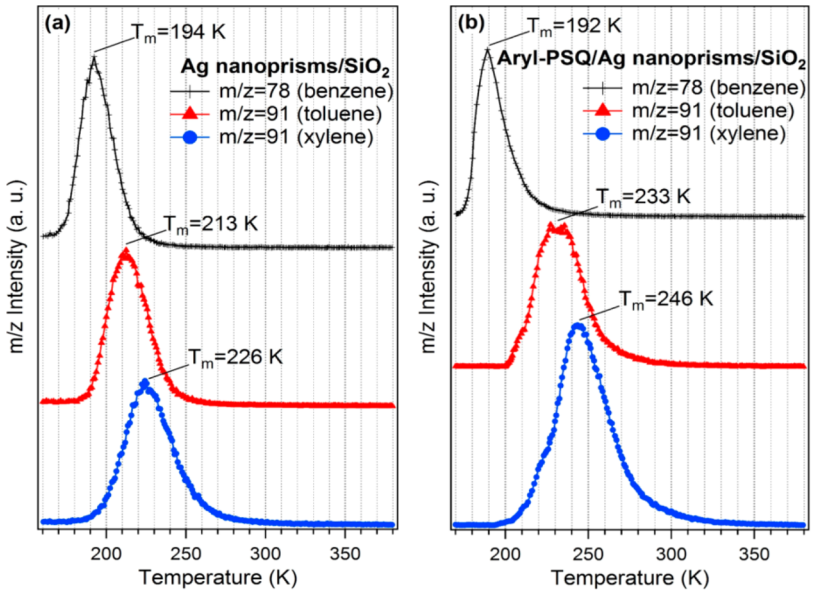

Figure 5. TPD spectra (β = 120 K/min) reporting desorption of xylene, toluene, and benzene from (a) Ag nanoprisms deposited on a SiO_2/stainless steel support and (b) a diph-PSQ film deposited on a Ag nanoprism/SiO_2/stainless steel support.

The largest absorbance difference is located at 653 nm, i.e., at a slightly larger wavelength with respect to the LSPR peak, in the region where the derivative of the curve is larger. At the wavelength where the difference is maximal, the change in absorbance was studied as a function of the refractive index variation. Figure 4b shows the change due to a variation of the refractive index (Δn) from −0.002 to 0.002. For such small variations, the dependence is linear, and the curve shows that even very small refractive index variations can be detected using the proposed strategy.

3.2. Ultra-High-Vacuum Temperature-Programmed Desorption Measurements. In Figure 5, we report the aromatic hydrocarbon desorption spectra from Ag nanoprism/SiO_2 (Figure 5a), taken as a reference measurement, to verify the interaction between the metal nanostructures and analytes, and from the sensor films (diph-PSQ film/Ag nanoprism/SiO_2) (Figure 5b). All TPD curves for benzene, toluene, and xylene exhibit a single peak, whose asymmetric shape confirms a first-order desorption process. By using the Redhead[28] approximation, it is possible to calculate the heat of desorption for each aromatic hydrocarbon; the numeric values are listed in Table 1.

Table 1. Desorption Heat Values for Benzene, Toluene, and Xylene from Ag Nanoprism/SiO_2 and diph-PSQ/Ag Nanoprism/SiO_2 Systems

	ΔE_d (kJ/mol) for the Ag nanoprism/SiO_2 system	ΔE_d (kJ/mol) for the diph-PSQ/Ag nanoprism/SiO_2 system
benzene	55 ± 3	55 ± 3
toluene	61 ± 3	67 ± 3
xylene	65 ± 3	71 ± 3

It is important to point out that the ΔE_d values for benzene on Ag [the Ag(111) surface was chosen as a prototype substrate] have already been calculated both experimentally[29] and theoretically,[30] resulting in values of 40.5 and 31.8 kJ/mol, respectively. Moreover, Caputo et al.,[30] by means of second-order Møller−Plesset perturbation theory (MP2), calculated the potential energy curve for benzene on Ag(111). This is a van der Waals type potential curve, with a shallow minimum at ∼3.5 Å, characteristic of a weak interaction involving the π system. This means that the interaction between aromatic hydrocarbons and Ag is largely dominated by van der Waals or dispersion forces. The ΔE_d values calculated for the Ag nanoprism/SiO_2 system (Table 1) are higher than expected for an adsorbate−Ag interaction and range from 55 to 65 kJ/mol. A careful comparison of our data with the literature suggests that the main desorption contributions we display in Figure 5a could be due to the interaction between the aromatic hydrocarbon π electrons and the SiO_2 substrate terminal silanol groups left uncovered.[31] The ΔE_d values reported for the interaction of benzene, toluene, and xylene with Si-OH-containing species are in the range of 50−70 kJ/mol, in agreement with our results.[32] Moreover, ΔE_d increases as a function of the number of methyl groups (-CH_3) in the benzene ring, which are known to be electron donors. The consequence is that the overall adsorbate π electron density increases as the number of -CH_3 groups increases. A higher π electron density favors the interaction with the substrate -OH groups, so that the ΔE_d values decrease in the following order: ΔE_d(xylene) > ΔE_d(toluene) > ΔE_d(benzene).

By comparison of the TPD spectra reported in panels a and b of Figure 5, it is clear that, with the exception of benzene, the deposition of a diph-PSQ film on the Ag nanoprism/SiO_2 substrate system causes a peak shift to a higher T_m. This means higher ΔE_d values for toluene and xylene (67.1 and 71.1 kJ/mol, respectively). In particular, with the change from benzene to toluene, ΔE_d increases by 22% (∼11% in the case of the Ag nanoprism/SiO_2 system) and by ∼6% from toluene to xylene (6% also in the case of the Ag nanoprism/SiO_2 system). This effect can be related to the presence of organic groups in the hybrid film, which are able to interact with the π electrons of toluene and xylene aromatic rings (π−π interaction), making the diph-PSQ film interact more with alkyl-substituted aromatic rings. As already shown for the aromatic hydrocarbon/Ag/SiO_2 system (Figure 5a), the presence of -CH_3 electron donor groups in the benzene ring increases the π electron density,

dx.doi.org/10.1021/am501042f | ACS Appl. Mater. Interfaces 2014, 6, 7773−7781

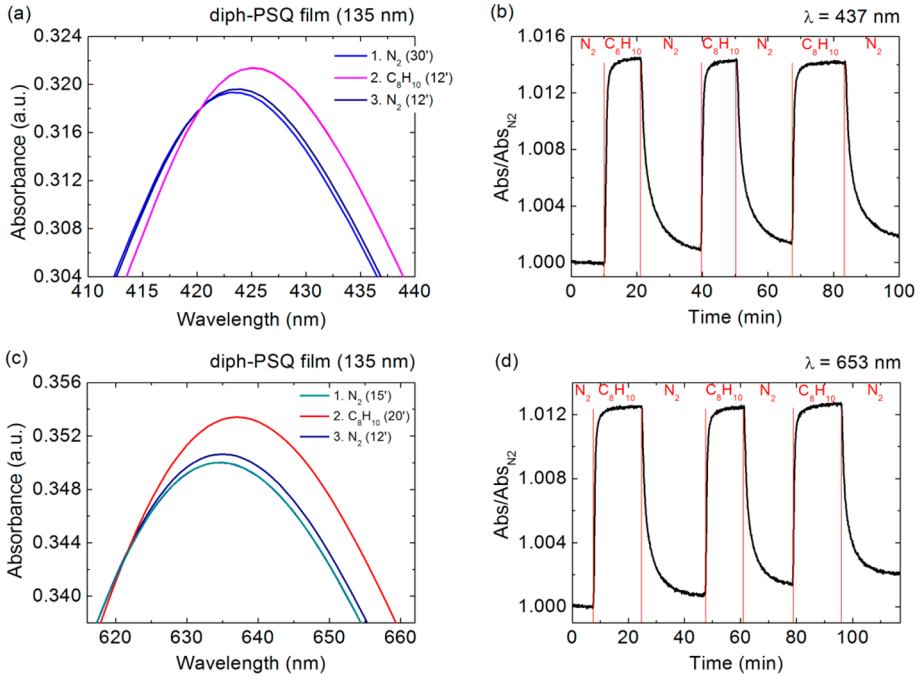

Figure 6. LSPR absorption bands and dynamic responses at fixed wavelengths, for a 135 nm thick diph-PSQ film coating a Ag nanoprism array deposited on a sodalime slab, under successive cycles of exposure to N_2 and 30 ppm xylene in N_2. For λ = 437 nm, t_{resp} = 80 s, t_{reg} = 12 min, and RI = 0.014. For λ = 653 nm, t_{resp} = 90 s, t_{reg} = 10 min, and RI = 0.012.

thus favoring the $\pi-\pi$ interaction with the aryl-PSQ film organic functional groups. Therefore, Ag nanoprisms embedded between the diph-PSQ film and SiO_2 do not play an active role in the interaction of the sensor with aromatic hydrocarbons, in contrast with previously reported results collected on a Au/diph-PSQ nanostructured plasmonic sensor.[22] In particular, the ΔE_d value calculated for the xylene−diph-PSQ complex becomes less intense, and this is probably due to the interaction between Ag (Ag nanoprisms embedded) and diph-PSQ organic groups.

3.3. Aromatic Hydrocarbon Sensing Measurements. To test the gas sensing performance, UV−vis absorption spectra of the sensors were recorded in the wavelength range of 300−900 nm, under successive cycles of exposure to N_2 and to the analytes for tens of minutes. Preliminary results pointed to the importance of performing a 30 min thermal annealing at 200 °C to optimize the performance of the sensors: response and regeneration kinetics were promoted, and the RI was generally increased by 1 order of magnitude (not shown). Such a pretreatment did not substantially alter the chemical or physical properties of the employed materials but favored outgassing and elimination of adsorbed species.

Let us take into consideration a sensor made by a 135 nm thick diph-PSQ film deposited on a Ag nanoprism array, annealed at 200 °C for 30 min (Figure 6).

Panels a and c of Figure 6 report in detail the LSPR curves characterizing such a device when the sensor made contact with two different environments: carrier and 30 ppm xylene in N_2. In the presence of xylene molecules, the intensities of the resonances increased and the resonances were red-shifted. An increase in the refractive index of the dielectric, as a consequence of the sol−gel film−xylene coupling, might determine the resonance shift to lower frequencies. For λ = 437 nm, t_{resp} = 80 s, t_{reg} = 12 min, and RI = 0.014, while for λ = 653 nm, t_{resp} = 90 s, t_{reg} = 10 min, and RI = 0.012.

To confirm that Ag nanoprism arrays do not play a direct active role as selective sensing elements for aromatic hydrocarbons, a gas sensing test was performed, without depositing the active functional layer. Figure 7 shows the absence of a response to 30 ppm xylene, for two λ values of the incident light, exciting two different LSPR multipolarities.

In Figure 8, the results of time-resolved sensing tests performed at a fixed λ wavelength, within the LSPR range, are shown for a 65 nm thick diph-PSQ film. The dynamic response is characterized by a t_{resp} of 3 min, a t_{reg} of 20 min, and an RI of 0.0124 for xylene; a t_{resp} of 106 s, a treg of 6 min, and an RI of 0.0060 for toluene; and a t_{resp} of 35 s, a t_{reg} of 95 s, and an RI of 0.0015 for benzene. The RI is not lower for thinner sol−gel films, as long as the sensing film extends for almost the whole penetration depth of the plasmonic field. Indeed, FEM simulations indicate that the local fields have a decay length of ∼15 nm in the gap region between two nanoprisms ($x-y$ plane) and of ∼20 nm along the vertical direction, z. The dynamics is faster, at the expense of a lower RI, for molecules presenting a smaller number of methyl substituents and less steric hindrance. Thus, $RI_{d\text{-}(xylene)} > RI_{d\text{-}(toluene)} > RI_{d\text{-}(benzene)}$, which is consistent with the trend in ΔE_d obtained from UHV-TPD measurements. Experimental data show that, after a cycle of response and regeneration, the baseline level is not always recovered within the error, and such an effect is more evident when the response intensity is low (comparable with the baseline drift). This behaviour can be ascribed to experimental factors, taking into account that data were acquired at room temperature.

Other time-resolved sensing tests were performed on sensors in which the capture component was made by ph-PSQ films, deposited on Ag nanoprism arrays. Figure 9 reports the UV−vis absorption spectra characterizing a sensor made of a 200 nm thick ph-PSQ film coating a Ag nanoprism array deposited on a sodalime slab, and the dynamic response, under successive

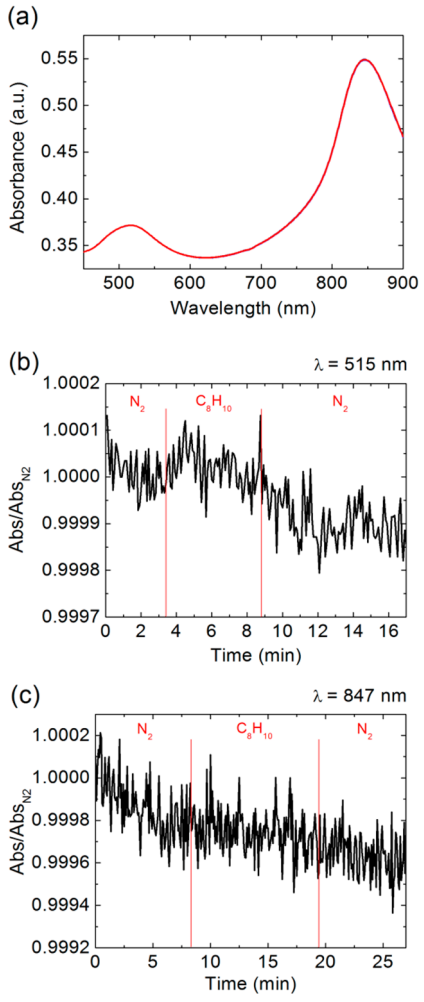

Figure 7. LSPR absorption bands and dynamic responses at two fixed wavelengths, for a Ag nanoprism array deposited on a sodalime slab (without any functional sol−gel coating), under successive cycles of exposure to N_2 and 30 ppm xylene in N_2. The system does not respond.

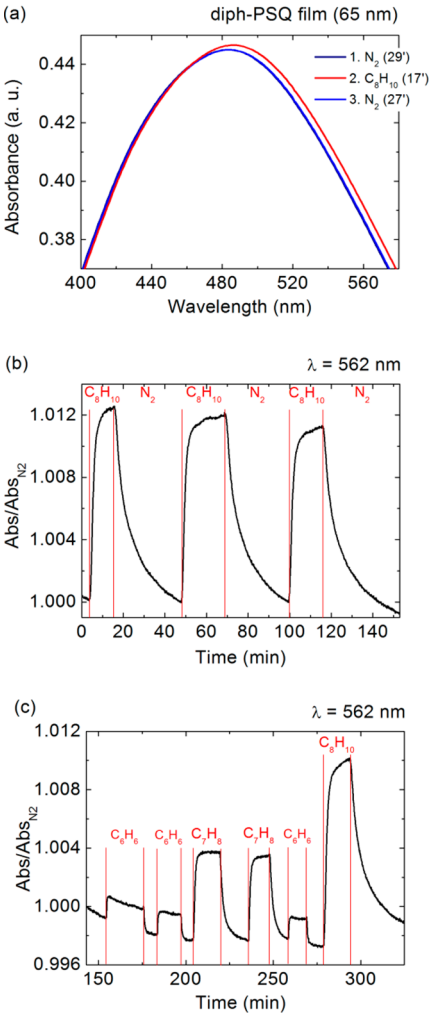

Figure 8. LSPR absorption bands and dynamic responses at λ = 562 nm, for a 65 nm thick diph-PSQ film coating a Ag nanoprism array deposited on a sodalime slab, under successive cycles of exposure to N_2 and the analytes. An annealing step at 200 °C for 30 min was applied before sensing measurements. For xylene, t_{resp} = 3 min, t_{reg} = 20 min, and RI = 0.0124. For toluene, t_{resp} = 106 s, t_{reg} = 6 min, and RI = 0.0060. For benzene, t_{resp} = 35 s, t_{reg} = 95 s, and RI = 0.0015.

cycles of exposure to N_2 and xylene, successively exciting the three LSPRs. For λ = 478 nm, t_{resp} = 275 s, t_{reg} = 13 min, and RI = 0.0037. For λ = 656 nm, t_{resp} = 223 s, t_{reg} = 24 min, and RI = 0.0235. For λ = 880 nm, t_{resp} = 4 min, t_{reg} = 11 min, and RI = 0.0049.

In general, we found that the RI and response time are not very sensitive to the particular multipolarity used: the most important parameter for having a better signal-to-noise ratio is the intensity of the resonance used. The slower sensor dynamics, in this case of ph-PSQ, can be ascribed to the higher expected diffusion times, because of the lower aperture degree of the sol−gel hybrid network, with respect to diph-PSQs, which is conferred by one bridging benzene ring (instead of a chain of two benzenes for diph-PSQs). Moreover, a comparison between the RI of a Ag/ph-PSQ sensor with a Ag/diph-PSQ-based sensor (given a similar LSPR amplitude, and sensing layer thickness extending through the whole plasmonic field) confirms evidence revealed by previous gas sensing measurements:[22] ph-PSQ films are sensitive layers guaranteeing RI values higher than those of diph-PSQ films, at the expense of longer response and regeneration times.

A calibration curve for the three gases is given in Figure 10, reporting the RI values versus gas concentration in the range of 5.5−30.0 ppm, for a 150 nm thick sensor that consists of a diph-PSQ film deposited on a Ag nanoprism array. The responses are linear within the experimental errors. The sensitivity, evaluated as $\Delta RI/\Delta c$, where c is the concentration of the analyte, is $(3.6 \pm 0.2) \times 10^{-4}$ ppm^{-1} for xylene, $(2.1 \pm 0.1) \times 10^{-4}$ ppm^{-1} for toluene, and $(1.4 \pm 0.1) \times 10^{-4}$ ppm^{-1} for benzene. The developed sensor is not able to discriminate in a mixture of gases the contribution of the single type of aromatic hydrocarbon; thus, the sensitivity to aromatic hydrocarbons is estimated to be $(1.4 \pm 0.1) \times 10^{-4}$ ppm^{-1}. Taking into consideration the same type of sensor (150 nm thick diph-PSQ film deposited on the Ag nanoprism array), the limit of detection for the sensor can be determined as the concentration of analyte that results in a sensor response equal to three standard deviations of the baseline noise. Thus, a threshold limit of detection of 0.3 ppm was estimated for xylene, 0.5 ppm for toluene, and 0.7 ppm for benzene, while the actual lowest measured concentration is 5.5 ppm for each gas.

Via correlation of results from experimental data with simulations for the Ag/diph-PSQ-based system, the highest

dx.doi.org/10.1021/am501042f | ACS Appl. Mater. Interfaces 2014, 6, 7773−7781

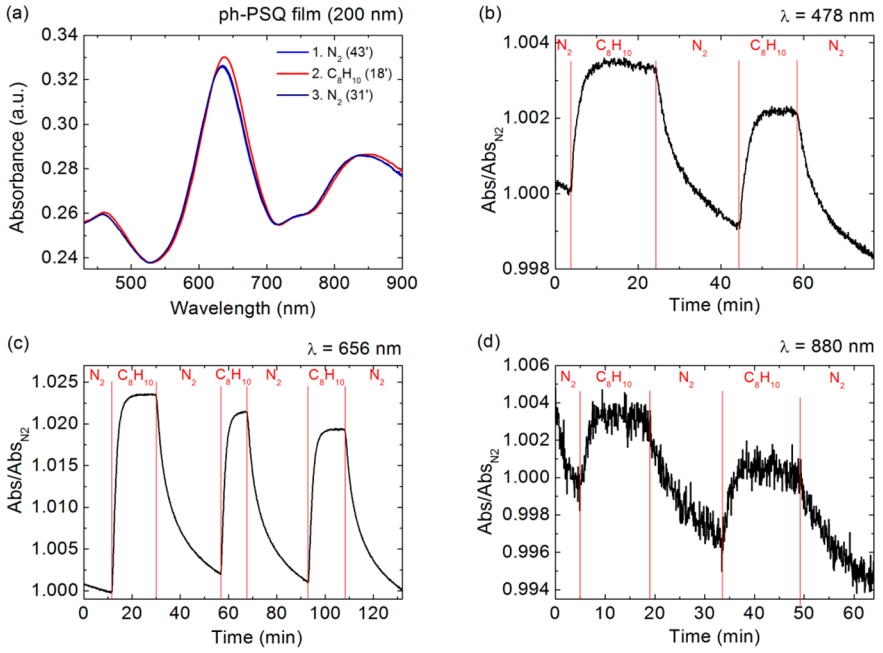

Figure 9. LSPR absorption bands and dynamic response at fixed wavelengths, for a 200 nm thick ph-PSQ film coating a Ag nanoprism array deposited on a sodalime slab, under successive cycles of exposure to N_2 and 30 ppm xylene in N_2. An annealing step at 200 °C for 30 min was applied before sensing measurements. For λ = 478 nm, t_{resp} = 275 s, t_{reg} = 13 min, and RI = 0.0037. For λ = 656 nm, t_{resp} = 223 s, t_{reg} = 24 min, and RI = 0.0235. For λ = 880 nm, t_{resp} = 4 min, t_{reg} = 11 min, and RI = 0.0049.

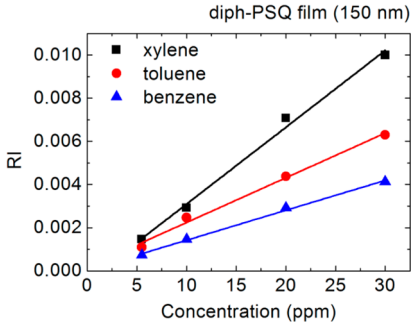

Figure 10. Calibration curves for a 150 nm thick diph-PSQ film coating a Ag nanoprism array deposited on a sodalime slab, under exposure to xylene, toluene, or benzene at concentrations in the range of 5.5−30.0 ppm. RI measurements where performed at λ = 556 nm, within a LSPR absorption band. The sensitivity is $(3.6 \pm 0.2) \times 10^{-4}$ ppm^{-1} for xylene, $(2.1 \pm 0.1) \times 10^{-4}$ ppm^{-1} for toluene, and $(1.4 \pm 0.1) \times 10^{-4}$ ppm^{-1} for benzene.

observed absorbance variation of 1.2% can be associated with a variation Δn of ∼0.001 of the functional film refractive index as a consequence to the interaction with 30 ppm xylene (Figure 4b). The possibility of detecting such a small variation in refractive index, caused by an interaction with the analyte, suggests the strong sensing capabilities of the presented technique.

4. CONCLUSIONS

LSPR sensors for aromatic hydrocarbons based on Ag nanoprism arrays coupled to aryl-PSQ thin films were designed and fabricated through a simple and inexpensive colloidal templating approach, followed by metal evaporation, and deposition of the functional sol−gel films. The sensors were tested against the detection of 30 ppm xylene, toluene, or benzene in N_2. Ultra-high-vacuum temperature-programmed desorption (UHV-TPD) measurements of the gas molecules on the Ag/diph-PSQ systems were conducted, resulting in an energy of interaction between the sensitive film and analytes in the range of 55−71 kJ/mol, increasing as a function of the number of electron-donating methyl substituents in the gas molecules.

The functional activity of the aromatic hydrocarbon gas optical sensors was tested by monitoring the LSPRs and was shown to be reversible. Response and regeneration times were shorter for sensors obtained exploiting diph-PSQ films as sensitive elements. Sensor dynamics was faster, at the expense of a lower RI, for gas molecules presenting a smaller number of methyl substituents and weaker steric hindrance, which is consistent with data obtained from UHV-TPD measurements. For Ag/diph-PSQ-based sensors, the highest observed absorbance variation of 1.2% could be associated, through finite element modeling (FEM), with a variation Δn of ∼0.001 of the functional film refractive index, as a consequence to the interaction with 30 ppm xylene. Among the different tested systems, the highest RIs were demonstrated for ph-PSQ films deposited on Ag nanoprism arrays, whereas the fastest response times were obtained in general from the thinnest films investigated.

AUTHOR INFORMATION

Corresponding Authors

*E-mail: laura.brigo@unipd.it (Laura Brigo). Phone: +39 049 8275023.

*E-mail: giovanna.brusatin@unipd.it (Giovanna Brusatin).

Author Contributions

L.B. and G.B. engineered the functional materials, performed the optical characterization of the plasmonic systems, and conceived, designed, and performed the sensing experiments. L.A., G.A.R., and G.G. performed TPD measurements and data analysis. N.M., C.S., and G.M. designed, simulated, and

fabricated the plasmonic substrates and performed SEM measurements. A.M. developed the gas sensing apparatus, supervised the gas sensing experiments, and helped in the interpretation of the gas sensing results. L.B., G.M., and L.A. wrote the manuscript.

Notes

The authors declare no competing financial interest.

■ ACKNOWLEDGMENTS

We acknowledge the University of Padova for funding through the PLATFORMS strategic project "PLAsmonic nano-Textured materials and architectures FOR enhanced Molecular Sensing" STPD089 KSC, coordinated by Prof. Massimo Guglielmi. Prof. Massimo Guglielmi is gratefully acknowledged for supervising the project work and for the very helpful discussions. We acknowledge the Italian Ministry of Education, University and Research (MIUR) for funding through the PRIN 2009 project "Novel plasmon-based processes and materials for sensor applications", coordinated by Prof. Renato Bozio, and FIRB Project RBAP115AYN.

■ REFERENCES

(1) Willets, K. A.; Van Duyne, R. P. Localized Surface Plasmon Resonance Spectroscopy and Sensing. *Annu. Rev. Phys. Chem.* **2007**, *58*, 267−297.
(2) Maier, S. A. *Plasmonics: Fundamentals and Applications*, 1st ed.; Springer: New York, 2007.
(3) Anker, J. N.; Paige Hall, W.; Lyandres, O.; Shah, N. C.; Zhao, J.; Van Duyne, R. P. Biosensing with Plasmonic Nanosensor. *Nat. Mater.* **2008**, *7*, 442−453.
(4) Homola, J. Surface Plasmon Resonance Sensors for Detection of Chemical and Biological Species. *Chem. Rev.* **2008**, *108*, 462−493.
(5) Haynes, C. L.; Van Duyne, R. P. Nanosphere Lithography: A Versatile Nanofabrication Tool for Studies of Size-Dependent Nanoparticle Optics. *J. Phys. Chem. B* **2001**, *105*, 5599−5611.
(6) Vogel, N.; Weissa, C. K.; Landfester, K. From Soft to Hard: The Generation of Functional and Complex Colloidal Monolayers for Nanolithography. *Soft Matter* **2012**, *8*, 4044−4061.
(7) Carpenter, M. A.; Mathur, S.; Kolmakov, A. *Metal Oxide Nanomaterials for Chemical Sensors*, 1st ed.; Springer: New York, 2013.
(8) Tran-Thi, T.-H.; Dagnelie, R.; Crunaire, S.; Nicole, L. Optical Chemical Sensors Based on Hybrid Organic−Inorganic Sol−Gel Nanoreactors. *Chem. Soc. Rev.* **2011**, *40*, 621−639.
(9) *2009 Guide to Occupational Exposure Values*, 1st ed.; ACGIH: Cincinnati, OH, 2008.
(10) Kim, H.-J.; Yoon, J.-W.; Choi, K.-I.; Jang, H. W.; Umar, A.; Lee, J.-H. Ultraselective and Sensitive Detection of Xylene and Toluene for Monitoring Indoor Air Pollution Using Cr-Doped NiO Hierarchical Nanostructures. *Nanoscale* **2013**, *5*, 7066−7073.
(11) Chatterjee, S.; Castro, M.; Feller, J. F. An E-Nose Made of Carbon Nanotube Based Quantum Resistive Sensors for the Detection of Eighteen Polar/Nonpolar VOC Biomarkers of Lung Cancer. *J. Mater. Chem. B* **2013**, *1*, 4563−4575.
(12) Hubálek, J.; Malysz, K.; Prášek, J.; Vilanova, X.; Ivanov, P.; Llobet, E.; Brezmes, J.; Correig, X.; Svěrák, Z. Pt-loaded Al_2O_3 Catalytic Filters for Screen-Printed WO_3 Sensors Highly Selective to Benzene. *Sens. Actuators, B* **2004**, *101*, 277−283.
(13) Hodgkinson, J.; Tatam, R. P. Optical Gas Sensing: A Review. *Meas. Sci. Technol.* **2013**, *24*, 012004.
(14) Bingham, J. M.; Anker, J. N.; Kreno, L. E.; Van Duyne, R. P. Gas Sensing with High-Resolution Localized Surface Plasmon Resonance Spectroscopy. *J. Am. Chem. Soc.* **2010**, *132*, 17358−17359.
(15) Loy, D. A.; Shea, K. J. Bridged Polysilsesquioxanes. Highly Porous Hybrid Organic-Inorganic Materials. *Chem. Rev.* **1995**, *95*, 1431−1442.
(16) Dąbrowski, A.; Barczak, M.; Robens, E.; Stolyarchuk, N. V.; Yurchenko, G. R.; Matkovskii, O. K.; Zub, Y. L. Ethylene and Phenylene Bridged Polysilsesquioxanes Functionalized by Amine and Thiol Groups as Adsorbents of Volatile Organic Compounds. *Appl. Surf. Sci.* **2007**, *253*, 5747−5751.
(17) Brigo, L.; Gazzola, E.; Cittadini, M.; Zilio, P.; Zacco, G.; Romanato, F.; Martucci, A.; Guglielmi, M.; Brusatin, G. Short and Long Range Surface Plasmon Polariton Waveguides for Xylene Sensing. *Nanotechnology* **2013**, *24*, 155502.
(18) Brigo, L.; Auzelyte, V.; Lister, K. A.; Brugger, J.; Brusatin, G. Phenyl-Bridged Polysilsesquioxane Positive and Negative Resist for Electron Beam Lithography. *Nanotechnology* **2012**, *23*, 325302.
(19) Brigo, L.; Grenci, G.; Carpentiero, A.; Pistore, A.; Tormen, M.; Guglielmi, M.; Brusatin, G. Positive Resist for UV and X-ray Lithography Synthesized Through Sol-Gel Chemistry. *J. Sol-Gel Sci. Technol.* **2011**, *60*, 400−407.
(20) Brigo, L.; Grenci, G.; Baù, L.; Carpentiero, A.; Mancin, F.; Romanato, F.; Tormen, M.; Guglielmi, M.; Brusatin, G. Hybrid Porous Resist with Sensing Functionality. *Microelectron. Eng.* **2011**, *88*, 1913−1916.
(21) Pistore, A.; Guglielmi, M.; Brusatin, G.; Kang, H. K.; Ferraris, C.; Romanato, F. Active Sol−Gel Thin Film on Nanostructured Plasmonic Surface. *Solid State Sci.* **2010**, *12*, 1898−1902.
(22) Brigo, L.; Cittadini, M.; Artiglia, L.; Rizzi, G. A.; Granozzi, G.; Guglielmi, M.; Martucci, A.; Brusatin, G. Xylene Sensing Properties of Aryl-Bridged Polysilsesquioxane Thin Films Coupled to Gold Nanoparticles. *J. Mater. Chem. C* **2013**, *1*, 4252−4260.
(23) Abdelghani, A.; Jaffrezic-Renault, N. SPR Fibre Sensor Sensitised by Fluorosiloxane Polymers. *Sens. Actuators, B* **2001**, *7*, 117−123.
(24) Chen, Y.-Q.; Lu, C.-J. Surface Modification on Silver Nanoparticles for Enhancing Vapor Selectivity of Localized Surface Plasmon Resonance Sensors. *Sens. Actuators, B* **2009**, *135*, 492−498.
(25) Hulteen, J. C.; Treichel, D. A.; Smith, M. T.; Duval, M. L.; Jensen, T. R.; Van Duyne, R. P. Nanosphere Lithography: Size-Tunable Silver Nanoparticle and Surface Cluster Arrays. *J. Phys. Chem. B* **1999**, *103*, 3854−3863.
(26) Jensen, T. R.; Duval Malinsky, M.; Haynes, C. L.; Van Duyne, R. P. Nanosphere Lithography: Tunable Localized Surface Plasmon Resonance Spectra of Silver Nanoparticles. *J. Phys. Chem. B* **2000**, *104*, 10549−10556.
(27) Jin, J.-M. *The Finite Element Method in Electromagnetics*, 2nd ed.; Wiley: New York, 2002.
(28) Redhead, P. A. Thermal Desorption of Gases. *Vacuum* **1962**, *12*, 203−211.
(29) Zhou, X.-L.; Castro, M. E.; White, J. M. Interactions of UV Photons and Low Energy Electrons with Chemisorbed Benzene on Ag(111). *Surf. Sci.* **1990**, *238*, 215−225.
(30) Caputo, R.; Prascher, B. P.; Staemmler, V.; Bagus, P. S.; Wöll, C. Adsorption of Benzene on Coinage Metals: A Theoretical Analysis Using Wavefunction-Based Methods. *J. Phys. Chem. A* **2007**, *111*, 12778−12784.
(31) Choudhary, V. R.; Mantri, K. Temperature Programmed Desorption of Toluene, p-Xylene, Mesitylene and Naphthalene on Mesoporous High Silica MCM-41 for Characterizing its Surface Properties and Measuring Heats of Adsorption. *Microporous Mesoporous Mater.* **2000**, *40*, 127−133.
(32) Choudhary, V. R.; Srinivasan, K. R.; Singh, A. P. Temperature-Programmed Desorption of Aromatic Hydrocarbons on Silicalite-I and ZSM-5-Type Zeolites. *Zeolites* **1990**, *10*, 16−20.